

1 A Lagrangian analysis of ice-supersaturated air over
2 the North Atlantic

E. A. Irvine,¹ B. J. Hoskins,^{1,2} K. P. Shine¹

Corresponding author: E. A. Irvine, Department of Meteorology, University of Reading, Earley Gate, Reading, RG6 6BB, UK. (e.a.irvine@reading.ac.uk)

¹Department of Meteorology, University of Reading, Reading, UK.

²Grantham Institute for Climate Change, Imperial College London, London, UK.

3 **Abstract.** Understanding the nature of air parcels that exhibit ice-supersaturation
4 is important because they are the regions of potential formation of both cir-
5 rus and aircraft contrails, which affect the radiation balance. Ice-supersaturated
6 air parcels in the upper troposphere and lower stratosphere over the North
7 Atlantic are investigated using Lagrangian trajectories. The trajectory cal-
8 culations use ERA-Interim data for three winter and three summer seasons,
9 resulting in approximately 200,000 trajectories with ice-supersaturation for
10 each season. For both summer and winter, the median duration of ice-supersaturation
11 along a trajectory is less than 6 hours. 5% of air which becomes ice-supersaturated
12 in the troposphere, and 23% of air which becomes ice-supersaturated in the
13 stratosphere will remain ice-supersaturated for at least 24 hours. Weighting
14 the ice-supersaturation duration with the observed frequency indicates the
15 likely overall importance of the longer duration ice-supersaturated trajec-
16 tories. Ice-supersaturated air parcels typically experience a decrease in mois-
17 ture content while ice-supersaturated, suggesting that cirrus clouds eventu-
18 ally form in the majority of such air. A comparison is made between short-
19 lived (less than 24 h) and long-lived (greater than 24 h) ice-supersaturated
20 air flows. For both air flows, ice-supersaturation occurs around the north-
21 ernmost part of the trajectory. Short-lived ice-supersaturated air flows show
22 no significant differences in speed or direction of movement to subsaturated
23 air parcels. However, long-lived ice-supersaturated air occurs in slower mov-
24 ing air flows, which implies that they are not associated with the fastest mov-
25 ing air through a jet stream.

1. Key points:

- 26 1. Ice-supersaturation in ERA-Interim is investigated using Lagrangian trajectories
- 27 2. The median duration of ice-supersaturation on trajectories is less than 6 hours
- 28 3. Long-lived ice-supersaturation occurs in slowly evolving synoptic flow

2. Introduction

29 The upper troposphere contains regions of ice-supersaturation (ISS), where the relative
30 humidity with respect to ice is above 100%, and the temperature is usually defined to be
31 less than 235 K to identify only regions of ice-phase and not mixed-phase [*Pruppacher*
32 *and Klett, 1997*]. These regions are interesting for two reasons. First, given sufficiently
33 high supersaturations, regions of ISS support the formation of natural cirrus clouds by
34 homogeneous freezing, or in some cases heterogeneous freezing (e.g. *Hoose and Möhler*
35 [2012]). Second, the occurrence of ice-supersaturated regions in the upper troposphere
36 and lower stratosphere coincides with the cruising altitude of commercial aircraft; aircraft
37 flying through these regions may form persistent contrails which may have a relatively
38 large, if uncertain, impact on climate [*Lee et al., 2009; Burkhardt and Kärcher, 2011*]. A
39 mean ISS of 15% has been observed in ice-supersaturated air in the upper-troposphere
40 [*Gierens et al., 1999*]; this is below the threshold for homogeneous freezing and therefore
41 persistent contrails may form in ice-supersaturated air that is free of natural cirrus cloud.

42 The global distribution of ice-supersaturated regions (ISSRs) can be derived from satel-
43 lite data, which show that globally, the maximum frequency of occurrence is in the tropics,
44 where it is related to the occurrence of deep convection. Tropical ISSRs are not consid-
45 ered in this paper, as they typically occur at altitudes higher than aircraft cruise altitudes.

46 In the mid-latitudes, high frequencies of supersaturation are coincident with the storm
47 track [*Spichtinger et al.*, 2003; *Lamquin et al.*, 2012]. ISSRs have also been diagnosed
48 using meteorological analyses, and their location linked to synoptic features. Using this
49 method, ISSRs have been found to preferentially occur in high pressure regions [*Imm-*
50 *ler et al.*, 2008; *Gierens and Brinkop*, 2012], in association with jet stream circulations
51 [*Irvine et al.*, 2012] and in warm conveyor belts associated with mid-latitude cyclones
52 [*Spichtinger et al.*, 2005a]. Generally, ISSRs occur in air that has experienced large-scale
53 upward and often divergent motion [*Kästner et al.*, 1999; *Gierens and Brinkop*, 2012], and
54 are thus both cooler and moister than surrounding subsaturated air [*Gierens et al.*, 1999;
55 *Spichtinger et al.*, 2003].

56 The location and duration of ISSRs is controlled by and evolves with the synoptic flow.
57 ISSRs identified from observations or synoptic charts give us an Eulerian view of ice-
58 supersaturation. However, ISSRs are dynamic features - air flowing through a synoptic
59 pattern forms part of the ISSR when it becomes saturated, and remains part of the ISSR
60 only while saturated (this perspective is discussed in *Spichtinger et al.* [2005a]; *Schumann*
61 [2012]). Therefore the timescales of an ISSR and an ice-supersaturated air parcel are
62 different, making it difficult to diagnose from a synoptic chart how long an air parcel will
63 remain ice-supersaturated, which is an important consideration if contrails form within
64 this air parcel. Contrails formed in cold ice-supersaturated air are advected with the air
65 parcel through a weather pattern and may last for many hours; contrail cirrus outbreaks
66 have been observed to persist for 12 -18 h [*Minnis et al.*, 1998; *Duda et al.*, 2004; *Haywood*
67 *et al.*, 2009].

68 The dynamic nature of ISSRs lends itself to an alternative approach for analysing these
69 regions, by using Lagrangian trajectories. This approach has previously been applied to
70 two case studies of ISS over Germany [*Spichtinger et al.*, 2005a, b], and for a cirrus cloud
71 in an ISSR [*Montoux et al.*, 2010]. Here, we extend this approach by using trajectories
72 to characterise air flows which lead to ISS in the North Atlantic region over multiple
73 seasons. We focus on understanding long-lived ice-supersaturated air flows, which may be
74 most important to understand from a radiative perspective as they can support long-lived
75 persistent contrails and also natural cirrus clouds.

76 The method for the calculation of the Lagrangian trajectories and that used to identify
77 ice-supersaturated air are presented in Section 3 together with an example for a synoptic
78 situation with strong ridging over the North Atlantic. Properties of the ice-supersaturated
79 air parcels are analysed in Section 4.1, including the duration of ISS, the spatial distri-
80 bution of ISS and the evolution of moisture along the trajectory. Differences between air
81 parcels which have long duration and short duration ISS, such as their direction and speed
82 of movement are analysed in Section 4.2, and conclusions are presented in Section 5.

3. Methodology

3.1. Description

83 Fully Lagrangian trajectories are calculated using an offline trajectory model [*Methven*,
84 1997; *Jackson et al.*, 2001], where the term offline means that the wind fields are ob-
85 tained directly from re-analysis data. The Lagrangian code uses a 4th order Runge-Kutta
86 integration with a 1 hour time step to calculate the trajectories. The horizontal wind
87 fields used to advect the air parcel are taken from the re-analysis data and the vertical
88 velocity is calculated using the continuity equation. Once the position of an air parcel

89 is calculated, the gridded re-analysis data are then interpolated to the current trajectory
90 location. The accuracy of the trajectory model has been examined for the extratropics in
91 *Methven et al.* [2003], and for the tropics in *Cau et al.* [2005].

92 The input meteorological data are 6-hourly European Centre for Medium-Range
93 Weather Forecasts Interim re-analysis data (ERA-Interim; *Dee et al.* [2011]) with hor-
94 izontal resolution T255 and 60 vertical levels. The parameterization of homogeneous
95 nucleation and ice-supersaturation in the model cloud scheme are described in *Tompkins*
96 *et al.* [2007]. In summary, the relative humidity over ice in the clear-sky portion of a
97 grid box is allowed to increase above 100%, up to a critical threshold. On reaching this
98 threshold, excess humidity is converted to ice and the in-cloud humidity adjusted back to
99 100%, within the model time-step.

100 Trajectories are released within the North Atlantic, defined to be the area 35-75 °N,
101 0-70 °W (shown on Figure 1(a)), on a grid with 1 ° horizontal spacing and from three
102 pressure levels: 300 hPa, 250 hPa and 200 hPa. We will refer to the time the trajectories
103 are initialised as $t=0$. From this grid, trajectories are calculated forwards in time to $t+48$
104 h and backwards in time to $t-48$ h, giving a complete trajectory length of 96 h.

105 Trajectories are initialised every 12 hours during three winters (December, January and
106 February) and three summers (June, July and August). The winters (starting December
107 1994, 1995 and 2003) and summers (1994, 1998 and 2006) were chosen for their different
108 North Atlantic Oscillation [*Barnston and Livezey, 1987*] behavior, in order to capture a
109 range of synoptic conditions over the North Atlantic. In total, the number of trajectories
110 calculated per season exceeds 4.6 million.

111 We use both relative humidity and temperature criteria to determine whether an air
112 parcel is within a region of ice-supersaturation. A criterion that the relative humidity
113 with respect to ice is above 98% is used. We take a threshold below 100% for two reasons.
114 Firstly, given the relatively coarse resolution of the ERA-Interim data, a grid box with a
115 grid mean humidity slightly below 100% is likely to contain some air parcels with humidity
116 above 100%, thus a threshold of 98% accounts for this subgrid-scale variability. Secondly,
117 to account for a bias from re-calculating the relative humidity from its temperature and
118 moisture fields, that is introduced by data interpolations onto different grids (personal
119 communication Paul Berrisford, ECMWF). In addition, consistent with previous studies
120 of ISS, we apply the criterion that the temperature should be below 235 K to avoid
121 identifying mixed-phase regions [*Pruppacher and Klett, 1997*]. The results presented in
122 this paper have been re-calculated with humidity thresholds of 95% and 100% and found
123 to be qualitatively similar. The main effect of using a modified humidity threshold is on
124 the number of ISS trajectories identified; for a threshold of 95% there is also a 6% increase
125 in the proportion of ISS trajectories with ISS duration of at least 24 h.

126 In this study we do not consider separately clear-sky and cloudy trajectories, since the
127 trajectories are calculated offline, and the information allowing us to distinguish such
128 trajectories is not available in the ERA-interim output. Interpolating a discontinuous
129 field such as cloud cover onto trajectories is problematic and we do not attempt to do
130 so. We note, however, that it is rare for trajectories to have achieved saturation with
131 respect to liquid water in the 18 hours preceding them becoming ice supersaturated.
132 In the one winter for which we assessed this, fewer than 1% of trajectories attained
133 a relative humidity of 80% with respect to liquid water (the threshold for stratiform

134 liquid water cloud formation in the ECMWF model [*Tiedtke, 1993*]) prior to attaining
135 ice-supersaturation.

136 Trajectories are released from multiple pressure levels. This could lead to a double-
137 counting of trajectories which rise from one level to another while the air is ice-
138 supersaturated. Occurrences of trajectories ascending from 300 - 250 hPa or 250 - 200
139 hPa whilst ice-supersaturated were found in fewer than 0.2% of winter trajectories. We
140 therefore assume this to have a negligible effect on our results. A second possibility, aris-
141 ing from releasing trajectories every 12 hours, is double-counting of trajectories where the
142 duration of ISS along the trajectory is greater than 12 hours. To avoid double-counting
143 ISS trajectories, we consider only those trajectories which meet the criteria for ISS at the
144 initial time ($t=0$). These trajectories are referred to as ISS trajectories; trajectories which
145 do not meet this criteria are considered as subsaturated trajectories (even if the criteria
146 are met at other points along the trajectory). Applying the above criteria results in a
147 total of 249,874 ISS trajectories in the winter data, and 188,895 in the summer data.

148 In our results we have divided the ISS trajectories into tropospheric and strato-
149 spheric. Ice-supersaturation has been observed to occur in the lower stratosphere near
150 the tropopause [*Gierens et al., 1999*]. However, the ISS in these regions is associated with
151 low temperatures and very low specific humidities compared to such regions in the tropo-
152 sphere [*Spichtinger et al., 2003*] and therefore the size of the radiative effect of contrails
153 which form in these regions is uncertain. In this study, a dynamic tropopause definition of
154 2 potential vorticity units (PVU) is used, which is appropriate for the range of latitudes
155 considered. We defined tropospheric ice-supersaturated air to be trajectories where the
156 first point of ISS is within the troposphere, (i.e. the potential vorticity at this point is

157 less than 2 PVU), and similarly for stratospheric air. In winter ice-supersaturation occurs
158 on 3.3% of stratospheric trajectories (1.6% for the summer data) which agrees well with
159 *Gierens et al.* [1999] who found ice-supersaturation in 2% of stratospheric data. Similarly,
160 ice-supersaturation occurs on 9.5% of tropospheric trajectories in winter, and 7% in sum-
161 mer. Because stratospheric ice-supersaturated air is often located close to the tropopause,
162 the partitioning of ISS air into tropospheric and stratospheric has some sensitivity to the
163 tropopause definition, particularly at high latitudes. It could be argued that a higher
164 threshold of 3 PVU or above may be preferable to define the tropopause at high latitudes
165 [*Zänagl and Hoinka, 2001*]; here we used a single tropopause definition, and note that us-
166 ing a tropopause definition of 3 PVU for the region north of 60°N reduces the amount of
167 ice-supersaturated air identified as stratospheric over Greenland.

3.2. Illustrative case study

168 As an illustration of the method used, we present a case study of trajectories initialised
169 within an ISSR. The synoptic pattern at 250 hPa is shown at $t=0$ (Figure 1(a)), cor-
170 responding to 1800 UTC 19 January 2004, when the trajectories were released. At this
171 time, there is strong ridging over the eastern North Atlantic, with a large region of ISS
172 just below the tropopause around the northern edge of the ridge. The 21 trajectories dis-
173 played on Figure 1 originated at 250 hPa from within this region of ISS (and within the
174 purple box on Figure 1(a)). The trajectories can be split into two broad groups according
175 to their pressure at $t-48$ h: one starting around 350 hPa (mostly the red trajectories on
176 Figure 1) and initially moving southwards and eastwards, and one starting around 600
177 hPa (mostly the blue trajectories on Figure 1) and ascending as they move northwards
178 and eastwards. Air moving northwards would be expected to ascend along isentropic sur-

179 faces; the increase in potential temperature (Figure 1(c)), accompanied by a decrease in
180 specific humidity from 4 g kg^{-1} to 0.5 g kg^{-1} (not shown), suggests release of latent heat
181 from condensation into cloud droplets during this ascent (note that clouds form when
182 the relative humidity criteria is reached locally, as defined by the parameterisation of the
183 sub-grid scale variability, and therefore cloud formation may occur when the grid-mean
184 humidity is substantially below the critical value [*Tompkins et al.*, 2007]). The ascent
185 around the ridge cools the air, leading to an increase in relative humidity (Figure 1(b)),
186 and the air attains ISS around the top of the ridge, and remains ISS until the air is forced
187 to descend (Figure 1(d)) as it begins to move southwards and warms. The small decrease
188 in potential temperature, of 1 K day^{-1} , (and negligible change in specific humidity, not
189 shown) whilst the air is supersaturated and in the upper troposphere is consistent with
190 typical radiative cooling rates. The time from the beginning to the end of the trajectories
191 is 96 h, showing that the large-scale synoptic trough-ridge pattern persisted during this
192 time. In this particular case study, the air only just attains ice-supersaturation; however,
193 high ice-supersaturations of up to 140% are observed in other cases.

194 The dynamic nature of ISSRs and the air which makes up these regions is illustrated by
195 considering their respective durations. The duration of ISS of an air parcel is defined as
196 the time period during which the air parcel is continually ice-supersaturated; the precision
197 of the calculation is therefore limited by the 6-hour time resolution of the meteorological
198 data. For example, an air parcel which is ice-supersaturated at a single point, $t=0$, along
199 a trajectory could be supersaturated for less than a single hour or just under 12 h (if
200 it becomes saturated just after $t-6$ and becomes subsaturated just before $t+6$). This is
201 likely to result in an over-estimate of the duration, therefore we take the minimum possible

202 time as the duration of ice-supersaturation: ISS at a single point is given a duration of
203 less than 6 h, at two consecutive points a duration of 6 h, at three consecutive points a
204 duration of 12 h and so on. Using this definition, for this case study, the duration of ISS
205 of the individual air parcels ranges from less than 6 hours (17 trajectories) to 12 hours (1
206 trajectory), although many remain close to saturation for 18 h; this is considerably less
207 than the duration of the ice-supersaturated region associated with the ridge. This region
208 of ISS was evident during the four days, 17-21 January 2004, that the ridge itself persisted
209 for, and disappeared only when the amplitude of the ridge had substantially decreased
210 (not shown).

4. Results

4.1. Properties of ISS trajectories

211 In this section the properties of the ISS trajectories, calculated for the three winters and
212 three summers discussed in Section 3, will be presented. Three properties are examined:
213 the duration of ISS of an air parcel, the spatial distribution of ISS and the evolution of
214 key variables while the air is ice-supersaturated.

215 A contrail formed in an ISS air parcel will be advected with the flow in that air parcel
216 (we assume any vertical motion of the contrail associated with falling ice-crystals will be
217 small), and therefore the duration of ISS is an upper-bound on the lifetime of a persistent
218 contrail. The duration of ISS along a trajectory is calculated by considering the number
219 of consecutive points of ISS along the trajectory, where the first point is obtained by
220 searching back in time from $t=0$, and the end point by searching forward in time from
221 $t=0$. This definition requires both relative humidity and temperature criteria to be met.
222 Note that a contrail, once formed, requires only the condition of relative humidity to

223 persist. Removing the temperature criterion did not significantly change the calculated
224 ISS durations.

225 The time resolution of the meteorological data used in the trajectory calculations is 6
226 hourly, which is insufficient to accurately determine the period for which an air parcel is
227 ice-supersaturated. It does, however, allow some general conclusions to be drawn. Pdfs
228 of the duration of ISS air (Figure 2) are non-Gaussian and highly-skewed towards shorter
229 durations. The median duration is less than 6 hours, i.e. ice-supersaturation was only
230 observed at a single point along the trajectory (at $t=0$). This is true for air parcels in both
231 summer and winter. The shape of the pdf is in agreement with previous studies of the
232 lifetime of satellite-observed linear contrails [Vazquez-Navarro, 2009], although we note
233 that the tail of the distribution is longer here than in Vazquez-Navarro [2009] probably
234 because the method detects contrails only whilst linear features and not once they have
235 spread into contrail-cirrus. It is also in agreement with the lifetime of modelled contrails
236 [Schumann, 2012], though care must be taken in the comparison since in Schumann [2012]
237 the lifetime of contrails is limited by sedimentation. Note that the lifetime of contrails
238 is generally smaller than that of the ice-supersaturated air parcel they form in, since as
239 noted by Schumann [2012] the air parcel must become saturated and then an aircraft must
240 fly through it to form the contrail. In addition loss processes, such as the sedimentation of
241 ice-particles may reduce the contrail optical depth leading to a subvisible contrail, before
242 the subsaturation of the ambient ice-supersaturated air.

243 The pdfs of ISS durations have a different shape for air which becomes ice-
244 supersaturated in the troposphere and air which becomes ice-supersaturated in the strato-
245 sphere. In winter, air which becomes ice-supersaturated in the stratosphere has a median

246 duration of 6h compared to less than 6h for tropospheric ISS air. A greater proportion
247 of stratospheric ISS air, 23% compared to 5% for tropospheric air, has a duration of ISS
248 of at least 24 h. In summer the difference is reduced; 11% of stratospheric ISS air and
249 5% of tropospheric ISS air have an ISS duration of at least 24 h. As noted in Section
250 3.1, the partitioning of ISS trajectories into tropospheric and stratospheric is sensitive to
251 the tropopause definition; however, we note that the proportion of ISS trajectories with
252 a lifetime of at least 24 h is increased by only a few percent if a tropopause definition of
253 3 PVU is used instead of the 2 PVU definition used here.

254 A contrail formed in an airmass for which the ISS duration is t_i is likely to persist for
255 a time of order t_i . If we consider that a longer-lived ISS air parcel is more likely (a) to
256 have an aircraft fly through it and (b) that a contrail formed within it will evolve into
257 contrail cirrus, then it is useful to have a measure of the overall longevity of each lifetime
258 category. This is calculated as $N_i t_i$, where N_i is the number of trajectories of a given
259 duration (from figures 2(a) and 2(c)). Since the units are time, we refer to this measure
260 as the total duration. The total duration is shown on Figure 2 (b) and (d). The shortest
261 (0-6 h) ISS duration, although the most frequent, does not contribute as much to the total
262 duration of ISS air as ISS trajectories which have a duration of 12 hours. The importance
263 of stratospheric ISS air is also evident; the total duration of stratospheric ISS air is larger
264 than that of tropospheric ISS air for durations greater than 18 h in winter. This shows
265 that the contribution of stratospheric ISS air may be significant, were contrails to form
266 in it because of its longer total duration, although other factors such as the temperature,
267 available moisture and natural cloud cover are also important in determining the radiative
268 effect of such contrails. However, in summer the proportion of ISS air in the stratosphere

269 is much smaller than in the troposphere due to both warmer air and a higher tropopause,
270 therefore tropospheric ISS air has a much greater total duration than stratospheric ISS
271 air. Figure 2 shows that the total duration of longer-lived ISS air is significant and hence
272 may be important in determining the contrail forcing. We will therefore give particular
273 attention to those ISS trajectories which have a long duration, defined here as continuous
274 ice-supersaturation for at least 24 h, under the assumption that these may be the most
275 important to understand.

276 The spatial distribution of the ISS start points, the location of air when it becomes ice-
277 supersaturated, is shown in Figure 3 for trajectories released on all 3 levels, for all three
278 years of data. The outline of the North Atlantic region that the trajectories were initialised
279 in is clearly visible, due to the short duration of ISS along most of the trajectories (Figure
280 2), so to first order Figure 3 shows the actual distribution of ISS in the upper troposphere
281 within this region. The distribution of ISS compares well to previous studies [*Spichtinger*
282 *et al.*, 2003; *Lamquin et al.*, 2012; *Irvine et al.*, 2012]. The distribution of ISS start points
283 in the troposphere in winter and summer is linked to the position of the jet stream,
284 which is generally further north in summer. For stratospheric ISS trajectories, there is a
285 maximum over Greenland in winter, which is largely absent in summer when the higher
286 tropopause results in a smaller proportion of ISS air in the stratosphere at the levels used
287 in this study. There is a northward shift in the position of tropospheric ISS trajectories
288 from winter to summer, which may be caused by both temperatures rising above the
289 threshold used to avoid identifying regions of mixed-phase and a northward shift in the
290 jet stream. The spatial distribution of long-lived ISS air is broadly similar to that of all

291 ISS air for tropospheric ISS air in both seasons, although fewer are associated with the
292 jet stream (Figure 3(a)).

293 The Lagrangian trajectories can be used to analyse the evolution of the moisture content,
294 pressure and temperature of an air parcel, to determine which has a greater control on the
295 duration of ISS. Previous studies have shown that adiabatic cooling of rising air is the main
296 pathway to ISS [*Gierens et al.*, 1999; *Spichtinger et al.*, 2005a], but it is unclear whether
297 it is a decrease in specific humidity from the formation and sedimentation of ice-crystals
298 or adiabatic compression of sinking air that have the biggest effect on the duration of ISS.
299 First, we analyse the evolution of the specific humidity of ice-supersaturated air. Pdfs of
300 the change in specific humidity and pressure during the period of ISS are shown in Figure
301 4, for trajectories where ISS is observed at a minimum of two consecutive points along
302 the trajectory (corresponding to a duration of at least 6 h). Specific humidity decreases
303 by up to 80% during the ISS duration (Figure 4(a)), while the air undergoes weak ascent
304 of typically less than 20 hPa (Figure 4(b)) at the same time. The decrease in specific
305 humidity during the period of ISS is consistent with condensation processes from cloud
306 formation, which suggests that cirrus cloud eventually forms in the majority of air masses
307 that become ice-supersaturated, although we lack the relevant model data to confirm
308 this. This would agree with lidar observations of ice-supersaturated regions which show
309 the majority of ice-supersaturated air also contains ice particles [*Immler et al.*, 2008], so
310 that contrails are often observed embedded in thin or subvisible cirrus [*Immler et al.*,
311 2008; *Voigt et al.*, 2010; *Iwabuchi et al.*, 2012]. To assess the importance of the changes
312 in specific humidity on the duration of ISS, we re-calculated the relative humidity at the
313 first point of subsaturation after the period of ISS, using (1) the specific humidity from

314 the last point of ISS and (2) the pressure and temperature from the last point of ISS,
315 for winter trajectories released from 250 hPa. For case (2) 60% of trajectories are now
316 ISS whereas for case (1) only 30% of trajectories are ISS. This suggests that adiabatic
317 compression of sinking air parcels is the major control on the duration of ISS of an air
318 parcel.

4.2. A comparison of short and long duration ISS air

319 In this section the recent history of air parcels is considered to determine differences
320 between airflows which lead to ice-supersaturation and those which do not. Differences
321 between the recent history of long-duration (at least 24 h) ISS air and shorter-duration
322 (less than 24 h) ISS air are also investigated to understand whether it might be possible
323 to know a priori whether an air parcel will remain in an ice-supersaturated state for
324 a significant period of time. This is important to understand from the perspective of
325 the formation of long-lived contrails in such air parcels and their possible evolution into
326 contrail cirrus.

327 The 24 h period leading up to ISS (or the 24 h period prior to $t=0$ for subsaturated air)
328 is used to investigate the recent history of supersaturated and subsaturated air masses.
329 Three variables are analysed: the speed of air and the change in pressure along a trajectory,
330 and the direction of movement. The speed of air along a trajectory is the wind speed in the
331 region of the trajectory, since the trajectories are calculated by using the horizontal wind
332 components to advect air parcels. Equally, the change in pressure along the trajectories
333 is the vertical motion of the ambient air, with negative values implying ascent. Pdfs of
334 wind speed and vertical motion are shown in Figure 5, for both ISS air and subsaturated
335 air, which is used as a climatology. In winter (Figure 5(a)), the speed of subsaturated air

336 has an approximately normal distribution, with a peak around 30 m s^{-1} and a tail out to
337 70 m s^{-1} indicative of air flowing through the jet stream. The pdf for shorter-lived ISS air
338 is almost identical to subsaturated air. In contrast, for long-lived ISS the distribution is
339 highly skewed towards smaller speeds with a peak at around 10 m s^{-1} . In summer (Figure
340 5(c)), the distribution of the speed of subsaturated air peaks at lower speeds of around
341 20 m s^{-1} and the tail cuts-off at smaller speeds than in winter. As for winter, long-lived
342 ISS air is associated with smaller wind speeds than shorter-lived ISS air, although the
343 difference is less-pronounced, due to the smaller range of wind speeds observed at these
344 altitudes in summer when the jet stream is weaker.

345 The distribution of the change in pressure along a trajectory peaks around zero for
346 subsaturated air, and contains both ascent and descent. In contrast, whilst pdfs for
347 both long and short-lived ISS air have a peak near zero ascent, they contain almost
348 no values of descent; as expected, both shorter-lived and long-lived ISS occurs in air
349 which has ascended. This is consistent with the assumption from *Gierens and Brinkop*
350 [2012] that the descent they found in pdfs of vertical velocity of ISSRs is associated with
351 decaying ISSRs. In winter, the distribution of pressure change for long-lived ISS air
352 has a peak at smaller values of ascent and a smaller variance compared to shorter-lived
353 ISS air (Figure 5(b)). In summer, the peak of both distributions are similar (Figure
354 5(d)), with larger frequencies of strong ascent for the shorter-lived ISS air. Considering
355 the distributions of speed and pressure change together, the slower wind speeds and
356 smaller ascent of long-lived ISS air suggest that it occurs in more slowly evolving weather
357 situations. The rate of change of temperature, pressure and specific humidity during the

358 period of ice-supersaturation is slower in longer-lived ISS trajectories (not shown), which
359 further supports this hypothesis.

360 Similarly, we can construct pdfs of the direction that the air moved in the 24 h leading
361 up to the first point of ISS, and the 24 h following the first point of ISS, for subsaturated
362 air (the climatology), shorter-lived and long-lived ISS air. Here, the results are split
363 by region, to allow for the different synoptic regimes which might influence the flow in
364 each region. Four sub-regions of interest are defined, based on the spatial distribution of
365 the ISS start points in Figure 3. We refer to these as: Atlantic-European, Mid-Atlantic,
366 Greenland and Iceland; their locations are shown as boxes on Figure 6(a). For each region,
367 we consider only those tropospheric ISS trajectories where the first point of ISS is within
368 the region of interest. Winter data is shown for all regions except Iceland, which has a
369 larger number of ISS points in summer.

370 An example of the movement of air along ISS trajectories is shown in Figure 6 for long-
371 lived tropospheric ISS air which becomes ice-supersaturated within the Atlantic-European
372 and mid-Atlantic regions. The location of these trajectories 24 h prior to becoming ice-
373 supersaturated within these regions, and their subsequent location 24 h later, gives an
374 indication of the synoptic conditions in which the ISS occurred. Air which becomes ice-
375 supersaturated over the Atlantic-European region comes predominantly from the west and
376 south-west (Figure 6(a)). However, air which becomes ice-supersaturated over the mid-
377 Atlantic region comes from a westerly direction (Figure 6(c)), and in general has moved
378 further than air which becomes ice-supersaturated over the Atlantic-European region,
379 suggesting the influence of the jet stream. 24 h after air becomes ice-supersaturated in
380 either region, when it is still supersaturated, it has moved towards the north and east.

381 In the case of persistent contrail formation within these air parcels, contrails which are
382 formed over the region of interest would be advected towards the north and east, to the
383 regions shown in Figure 6(b, d). This information can be summarised as pdfs to show the
384 movement of air leading up to and following ISS, for the different regions (Figures 7 and
385 8).

386 Pdfs of the direction of movement leading up to ISS are shown in Figure 7. For all
387 regions, the distributions for shorter-lived ISS air are similar to those for subsaturated
388 air, i.e. are similar to climatology. For the Atlantic-European region (Figure 7(a)) and
389 mid-Atlantic region (Figure 7(b)) in winter, which are dominated by the jet stream, flow
390 is predominantly from the west. However, the distribution for longer-lived ISS air shows
391 a higher proportion of southerly winds than subsaturated or shorter-lived ISS air. This
392 is also true for the Iceland region in summer (Figure 7(d)), where longer-lived ISS air
393 has a higher proportion of flow from the south-west than shorter-lived ISS air. For the
394 Greenland region in winter (Figure 7(c)), the distribution is broader, meaning that the
395 direction of flow is more variable. This region is generally north of the influence of the
396 jet stream and can have weak upper-level flow. For both Greenland and Iceland regions,
397 a greater proportion of the flow comes from an easterly direction.

398 Further information about the airflows leading to ISS is obtained by considering the
399 direction of flow during the 24 h following the first point of ISS. This is shown for all regions
400 in Figure 8. Once again the pdfs of direction of movement are similar for subsaturated air
401 and shorter-lived ISS air, indicating that using this method we cannot use flow direction
402 alone to distinguish between subsaturated and short-lived ISS air. For the Atlantic-
403 European and mid-Atlantic regions (Figures 8(a) and 8(b)), for subsaturated and short-

404 lived ISS air, the bulk of the pdf has shifted from flow from the south-west quadrant to
405 flow from the north-west quadrant. However, for long-lived ISS air the peak is from the
406 south-west, indicating that these airflows are still moving north (consistent with Figure
407 6(b)) and therefore likely to be experiencing ascent. If, we consider instead the direction
408 of flow in the 24 h following the last point of ISS (not shown), we find that the long-lived
409 ISS air now has a northerly component, consistent with the air descending and becoming
410 subsaturated. The difference between short and long-lived ISS airflows is less clear for
411 the Greenland and Iceland regions, as the variance of the pdfs is large indicating that the
412 flow direction is very variable in these regions.

413 Put together, these results suggest that ice-supersaturation occurs around the north-
414 ernmost part of the trajectory. This suggests that long-lived ISS air primarily occurs in
415 two different synoptic situations: slower-moving air ascending around the periphery of an
416 anticyclone, and air rising in the jet stream circulations (regions of ascent in the right jet
417 entrance and left jet exit), that are on the edge of the circulation rather than in the core
418 of the jet.

5. Conclusions

419 Ice-supersaturated air parcels have been analysed using Lagrangian trajectories over
420 the North Atlantic. These highlight the dynamical nature of ice-supersaturated regions
421 that can be readily diagnosed from observational data and meteorological analyses; here
422 we investigate the air which makes up these regions. Trajectories have been calculated
423 from ERA-Interim data for three winter and three summer seasons, giving a large data
424 sample of trajectories which contain ice-supersaturation.

425 The duration of ice-supersaturation is generally short-lived; the median duration of ISS
426 is less than 6 h for both winter and summer seasons. In winter, the median duration of
427 stratospheric ISS air is longer at 6 h, although this could be an artefact of the coarse
428 time resolution of the meteorological data. 5% of tropospheric ISS trajectories and 23%
429 of stratospheric ISS trajectories have a duration of at least 24 h. We note that, whilst the
430 partitioning of ISS trajectories into tropospheric and stratospheric has some sensitivity to
431 the tropopause definition, the effect on the distributions of the ISS duration is small. The
432 percentage of ISS air which remains in a supersaturated state for at least 24 h is higher
433 than previous studies of contrail lifetimes (e.g. *Schumann* [2012]). This is expected, since
434 the duration of ISS air is an upper-bound on the lifetime of a contrail forming in that
435 air mass, and loss processes such as sedimentation of ice crystals are not accounted for
436 here. Weighting the ice-supersaturation duration with the observed frequency indicates
437 the likely overall importance of the longer duration ice-supersaturated trajectories, which
438 are a focus of this study.

439 The evolution of the properties of the air parcel whilst it is supersaturated show that air
440 parcels continue to ascend whilst saturated, and lose moisture. The decrease in moisture
441 content could be explained by the formation of cirrus clouds in the ISS air. In this study
442 we have not considered the presence of natural cirrus clouds in the ice-supersaturated air.
443 To do so would require interpolating cloud cover fraction to the location of the trajectories,
444 which could introduce spurious results since cloud cover is not a continuous field. Whilst
445 our results seem to suggest that natural cirrus cloud would eventually form in the majority
446 of air parcels which remain supersaturated for a long period of time, further studies would

447 be required to confirm this. It is adiabatic compression of sinking air parcels rather than
448 loss of moisture which is the major control on the duration of ISS of an air parcel.

449 We have analysed the history of air masses to discern differences between subsaturated
450 air and ISS air of short and long duration. For both long and short-lived ISS, the airflow
451 leading to ice-supersaturation is predominantly westerly. However this turns from having
452 a southerly to northerly component after (the last point of) saturation, and only weak
453 ascent. This suggests that the ISS occurs around the northernmost part of the trajectory.
454 In general, long-lived trajectories exhibit different behaviour to shorter-lived trajectories;
455 they occur in slower moving air which is ascending more slowly which implies they are
456 not associated with fast (or the fastest) moving air through a jet stream. The direction of
457 air leading up to ISS also shows a higher proportion of southerly winds than climatology,
458 and the air continues to have a northward component and rise whilst saturated. However,
459 considering the recent history (the previous 24 h) of short-duration ISS air and subsatu-
460 rated air the only difference is that subsaturated air may experience descent in its recent
461 history, whereas short-lived ISS air does not.

462 Lagrangian trajectories provide a dynamical perspective on ice-supersaturated air, and
463 have previously only been used in a case study approach. Here we have extended their
464 use to calculate trajectories for extended periods, to obtain a large sample of trajectories
465 containing ice-supersaturation. The trajectories are useful as an upper-bound of the
466 duration of potential contrails forming within ice-supersaturated air parcels, however they
467 are subject to the limits of the models capability to represent ice-supersaturation. In this
468 study we have not tried to separate out ISS trajectories into different weather situations,
469 to explain the variety of contrail durations. The results of this study suggest that at

470 least long-lived ISS occurs preferentially in some airflows but fails to discern differences
471 between short-lived ISS and subsaturated airflows, beyond confirming that ISS air occurs
472 in rising airflows. These results contribute to a better understanding of the dynamical
473 nature of ice-supersaturated regions which is important for evaluating predictions of ice-
474 supersaturation from numerical weather prediction or climate models.

475 **Acknowledgments.** This work is part of the REACT4C project, funded under the
476 EU 7th framework programme, grant ACP8-GA-2009-233772. The Lagrangian trajectory
477 code was provided by John Methven. We thank Klaus Gierens and John Methven for
478 comments on an earlier draft of the paper. We thank three anonymous reviewers for their
479 comments which helped to improve the manuscript.

References

- 480 Barnston, A. G., and R. E. Livezey (1987), Classification, seasonality and persistence of
481 low-frequency atmospheric circulation patterns, *Mon. Wea. Rev.*, *115*, 1083–1126.
- 482 Burkhardt, U., and B. Kärcher (2011), Global radiative forcing from contrail cirrus, *Nature*
483 *Climate Change*, *1*, 54–58, doi:10.1038/nclimate1068.
- 484 Cau, P., J. Methven, and B. J. Hoskins (2005), Representation of dry tropical layers and
485 their origins in ERA-40 data, *J. Geophys. Res.*, *110*, D06,110.
- 486 Dee, D. P. et al. (2011), The ERA-Interim reanalysis: configuration and performance of
487 the data assimilation system, *Q. J. R. Meteorol. Soc.*, *137*, 553–597, doi: 10.1002/qj.828.
- 488 Duda, D. P., P. Minnis, L. Nguyen, and R. Palikonda (2004), A case study of the de-
489 velopment of contrail clusters over the Great Lakes, *J. Atmos. Sci.*, *61*, 1132–1146,
490 doi:10.1175/1520-0469(2004)061.

- 491 Gierens, K., and S. Brinkop (2012), Dynamical characteristics of ice-supersaturated re-
492 gions, *Atmos. Chem. Phys.*, *12*, 11,933–11,942, doi:10.5194/acp-12-11933-2012.
- 493 Gierens, K. M., U. Schumann, H. G. J. Smit, M. Helten, and A. Marenco (1999), A
494 distribution law for relative humidity in the upper troposphere and lower stratosphere
495 derived from three years of MOZAIC measurements, *Ann. Geophysicae*, *17*, 1218–1226,
496 doi:10.1007/s00585-999-1218-7.
- 497 Haywood, J. M., R. P. Allan, J. Bornemann, P. M. Forster, P. N. Francis, S. Milton,
498 G. Rädcl, A. Rap, K. P. Shine, and R. Thorpe (2009), A case study of the radiative
499 forcing of persistent contrails evolving into contrail-induced cirrus, *J. Geophys. Res.*,
500 *114*, D24,201, doi:10.1029/2009JD012650.
- 501 Hoose, C., and O. Möhler (2012), Heterogeneous ice nucleation on atmospheric aerosols:
502 a review of results from laboratory experiments, *Atmos. Chem. Phys.*, *12*, 9817–9854,
503 doi:10.5194/acp-12-9817-2012.
- 504 Immler, F., R. Treffeisen, D. Engelbart, K. Krüger, and O. Schrems (2008), Cirrus, con-
505 trails, and ice supersaturated regions in high pressure systems at northern mid-latitudes,
506 *Atmos. Chem. Phys.*, *8*, 1689–1699, doi:10.5194/acp-8-1689-2008.
- 507 Irvine, E. A., B. J. Hoskins, and K. P. Shine (2012), The dependence of contrail formation
508 on the weather pattern and altitude in the North Atlantic, *Geophys. Res. Lett.*, *39*,
509 L12,802, doi:10.1029/2012GL051909.
- 510 Iwabuchi, H., P. Yang, K. N. Liou, and P. Minnis (2012), Physical and optical properties
511 of persistent contrails: climatology and interpretation, *J. Geophys. Res.*, *117*, D06,215,
512 doi:10.1029/2011JD017020.

- 513 Jackson, D. R., J. Methven, and V. Pope (2001), Transport in the low latitude tropopause
514 zone diagnosed using particle trajectories, *J. Atmos. Sci.*, *58*, 173–192.
- 515 Kästner, M., R. Meyer, and P. Wendling (1999), Influence of weather conditions on the
516 distribution of persistent contrails, *Meteorol. Appl.*, *6*, 261–271.
- 517 Lamquin, N., C. J. Stubenrauch, K. Gierens, U. Burkhardt, and H. Smit (2012), A global
518 climatology of upper-tropospheric ice supersaturation occurrence inferred from the At-
519 mospheric Infrared Sounder calibrated by MOZAIC, *Atmos. Chem. Phys.*, *12*, 381–405,
520 doi:10.5194/acp-12-381-2012.
- 521 Lee, D. S., D. W. Fahey, P. M. Forster, P. J. Newton, R. C. N. Wit, L. L. Lim, B. Owen,
522 and R. Sausen (2009), Aviation and global climate change in the 21st century, *Atmo-
523 spheric Environment*, *43*, 3520–3537, doi:10.1016/j.atmosenv.2009.04.024.
- 524 Methven, J. (1997), Offline trajectories: calculation and accuracy, *Tech. Report 44*, U. K.
525 *Univ. Global Atmos. Modelling Programme*, 18pp.
- 526 Methven, J., S. R. Arnold, F. M. O’Connor, H. Barjat, K. Dewey, J. Kent, and N. Brough
527 (2003), Estimating photochemically produced ozone throughout a domain using flight
528 data and a Lagrangian model, *J. Geophys. Res.*, *108*, D94,271.
- 529 Minnis, P., D. F. Young, D. P. Garber, L. Nguyen, W. L. Smith Jr., and R. Palikonda
530 (1998), Transformation of contrails into cirrus during SUCCESS, *Geophys. Res. Lett.*,
531 *25*, 1157–1160, doi: 10.1029/97GL03314.
- 532 Montoux, N., P. Keckhut, A. Hauchecorne, J. Jumelet, H. Brogniez, and C. David
533 (2010), Isentropic modelling of a cirrus cloud event observed in the midlati-
534 tude upper troposphere and lower stratosphere, *J. Geophys. Res.*, *115*, D02,202,
535 doi:10.1029/2009JD011981.

- 536 Pruppacher, H. R., and J. D. Klett (1997), *Microphysics of Clouds and Precipitation*,
537 Atmospheric and Oceanographic Sciences Library, Kluwer Academic Publishers, Dor-
538 drecht, The Netherlands.
- 539 Schumann, U. (2012), A contrail cirrus prediction model, *Geosci. Model Dev.*, 5, 543–580,
540 doi: 10.5194/gmd-5-543-2012.
- 541 Spichtinger, P., K. Gierens, and W. Read (2003), The global distribution of ice-
542 supersaturated regions as seen by the microwave limb sounder, *Q. J. R. Meteorol. Soc.*,
543 129, 3391–3410, doi: 10.1256/qj.02.141.
- 544 Spichtinger, P., K. Gierens, and H. Wernli (2005a), A case study on the formation and
545 evolution of ice supersaturation in the vicinity of a warm conveyor belt’s outflow region,
546 *Atmos. Chem. Phys.*, 5, 973–987, doi:10.5194/acp-5-973-2005.
- 547 Spichtinger, P., K. Gierens, and A. Dörnbrack (2005b), Formation of ice supersaturation
548 by mesoscale gravity waves, *Atmos. Chem. Phys.*, 5, 1243–1255, doi:10.5194/acp-5-1243-
549 2005.
- 550 Tiedtke, M. (1993), Representation of clouds in large scale models, *Mon. Wea. Rev.*, 121,
551 3040–3061.
- 552 Tompkins, A. M., K. Gierens, and G. Rädcl (2007), Ice supersaturation in the ECMWF
553 integrated forecast system, *Q. J. R. Meteorol. Soc.*, 133, 53–63, doi:10.1002/qj.14.
- 554 Vazquez-Navarro, M. R. (2009), Life cycle of contrails from a time series of geostationary
555 satellite images, *PhD Thesis, Deutsches Zentrum für Luft und Raumfahrt*.
- 556 Voigt, C., U. Schumann, T. Jurkat, D. Schauble, H. Schlager, A. Petzold, J.-F. Gayet,
557 M. Kramer, J. Schneider, S. Borrmann, J. Schmale, P. Jessberger, T. Hamburger,
558 M. Lichtenstern, M. Scheibe, C. Gournbeyre, J. Meyer, M. Kubbeler, W. Frey, H. Ka-

559 lesse, T. Butler, M. G. Lawrence, F. Holzapfel, F. Arnold, M. Wendisch, A. Doppelheuer,
560 K. Gottschaldt, R. Baumann, M. Zoger, I. Solch, M. Rautenhaus, and A. Dornbrack
561 (2010), In-situ observations of young contrails - overview and selected results from the
562 concert campaign, *Atmos. Chem. Phys*, *10*, 9039–9056, doi: 10.5194/acp-10-9039-2010.
563 Zängl, G., and K. P. Hoinka (2001), The tropopause in the Polar regions, *J. Clim.*, *14*,
564 3117–3139, doi: 10.1175/1520-0442(2001)014.

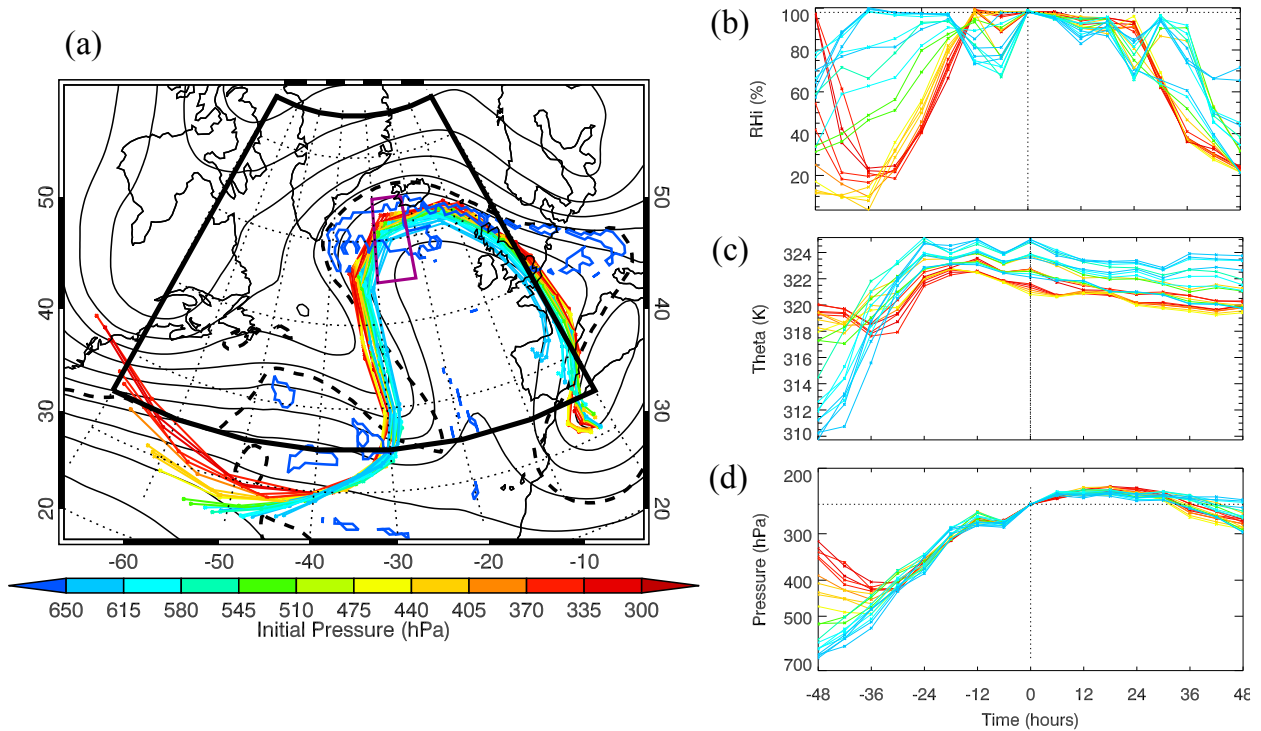


Figure 1. (a) An example of trajectories initialised within the purple box at 250 hPa; only trajectories which were within the ice-supersaturated region within this box (blue contours) are shown. The trajectories are released at $t=0$, corresponding to 1800 UTC 19 January 2004. The synoptic pattern at this time is shown by the 250 hPa geopotential height (thin black contours), the dynamical tropopause is displayed using the 2 PVU contour (thick dashed black line) and regions of ice-supersaturation at 250 hPa are outlined in blue. The path of the ISS trajectories is shown from $t-48$ to $t+48$, colored by the pressure of the air at $t-48$. The black box defines the north Atlantic region that the trajectories used in this study were initialised in. For the same period, (b) the relative humidity calculated with respect to ice, (c) potential temperature (theta) and (d) pressure along the trajectories.

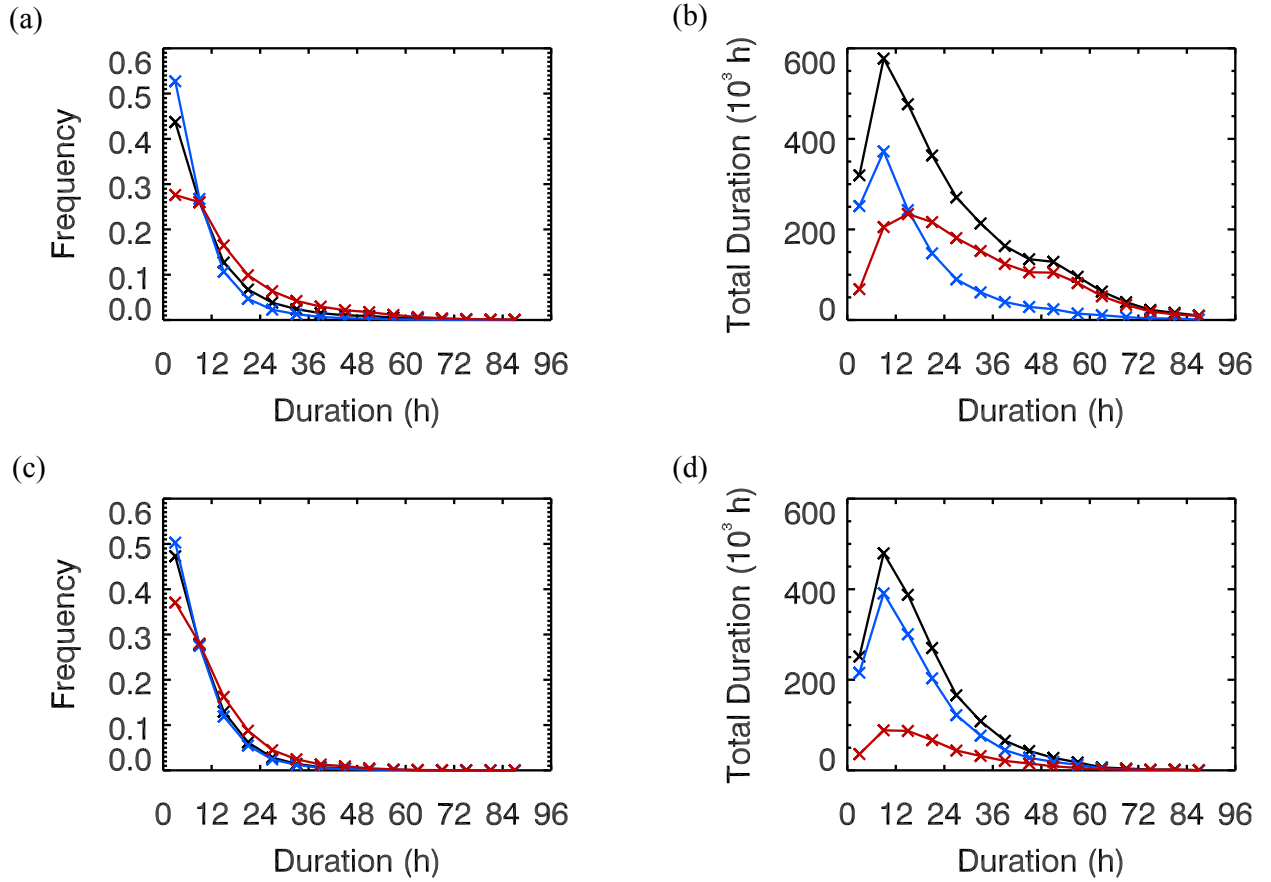


Figure 2. Histograms of the duration of ice-supersaturation calculated along air parcel trajectories, for trajectories released from all three pressure levels for (a) all three winters and (c) all three summers, using duration bins of 6 h. The three lines correspond to all ISS trajectories (black), tropospheric ISS air (blue) and stratospheric ISS air (red). Histograms of the total duration in units of 10^3 h, calculated for each duration bin as the median duration multiplied by the number of trajectories with that duration, (b) for winter and (d) for summer.

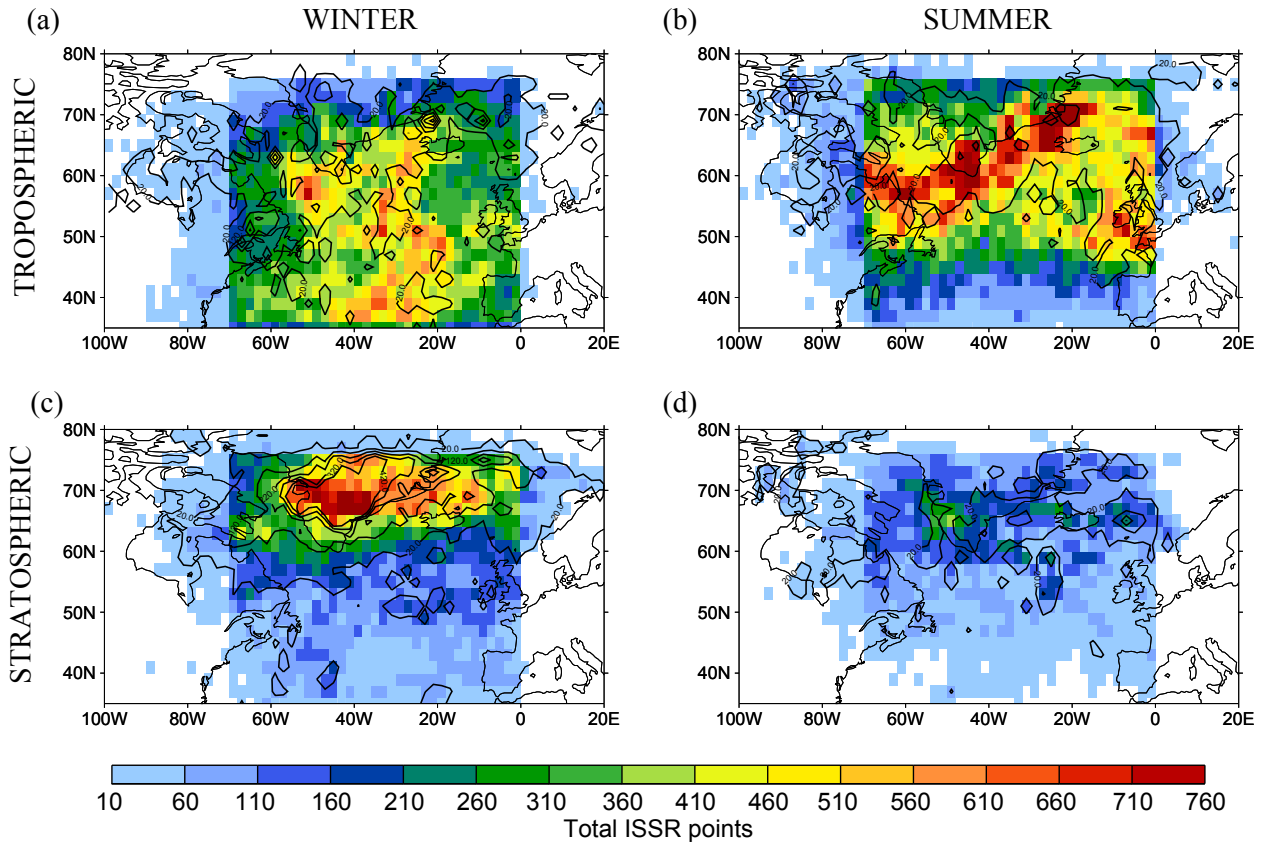


Figure 3. Map of the density of points where air first becomes ISS along a trajectory for all trajectories (colors) and long-lived ISS air (black contours) for (a) tropospheric winter, (b) tropospheric summer, (c) stratospheric winter and (d) stratospheric summer trajectories. Data have been gridded into 2° boxes before plotting. The minimum values of the line contours for long-lived ISS air is 20 with an interval of 100 trajectories.

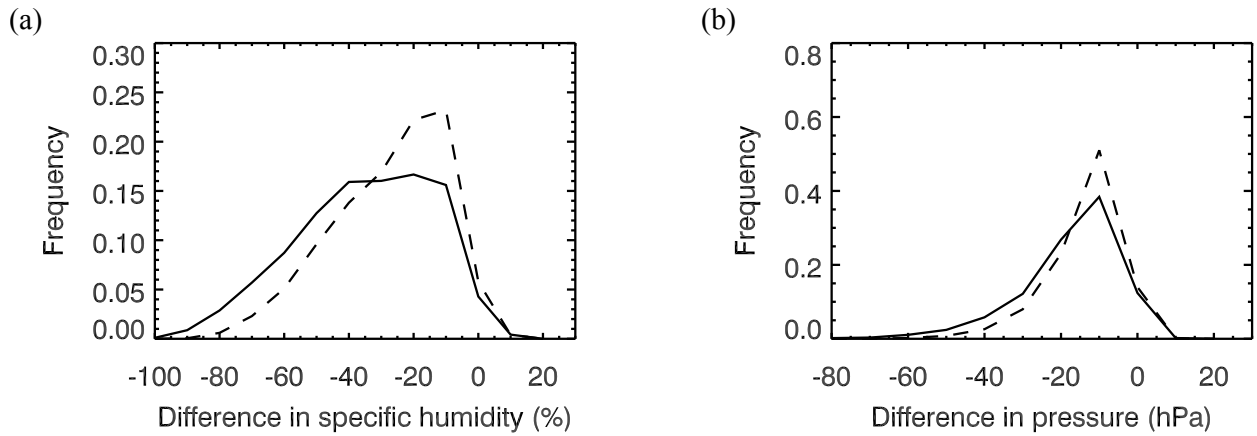


Figure 4. Change in (a) specific humidity and (b) pressure between the last point of ISS and first point of ISS along ISS trajectories released from 250 hPa in winter (solid line) and summer (dashed line). Negative changes in specific humidity indicate drying and negative changes in pressure indicate ascent during the period of ISS.

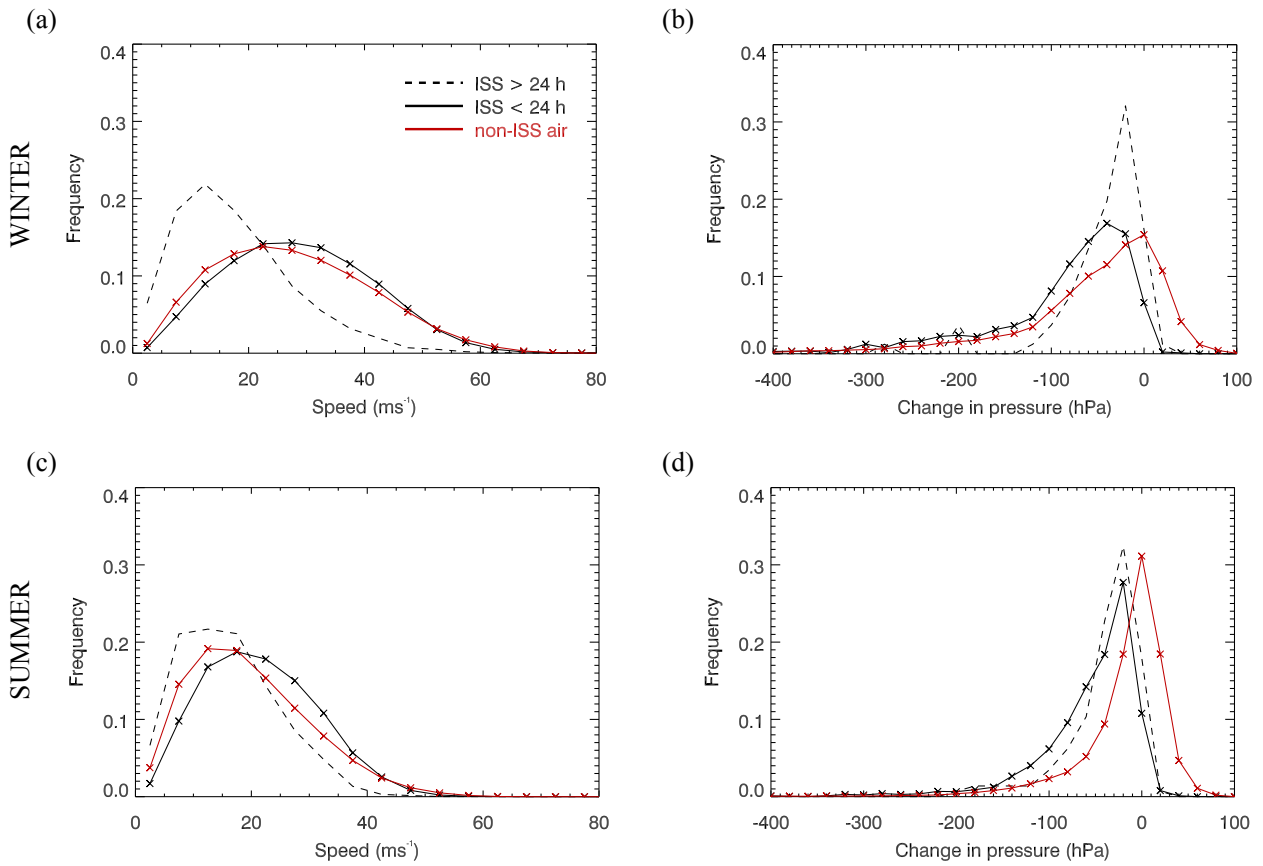


Figure 5. For the 24 h period prior to air becoming ISS, (a) the speed of air and (b) the change in pressure along the trajectory, for winter trajectories released from all three levels. (c), (d) as for (a), (b) but for summer trajectories. Change in pressure calculated as the pressure at the time the air parcel becomes supersaturated minus the pressure 24 hrs prior to this. Negative values imply parcel ascent. Shown for: tropospheric ISS air with a lifetime less than 24 h (black solid line), tropospheric ISS air with a lifetime of at least 24 h (black dashed line) and subsaturated air (red line).

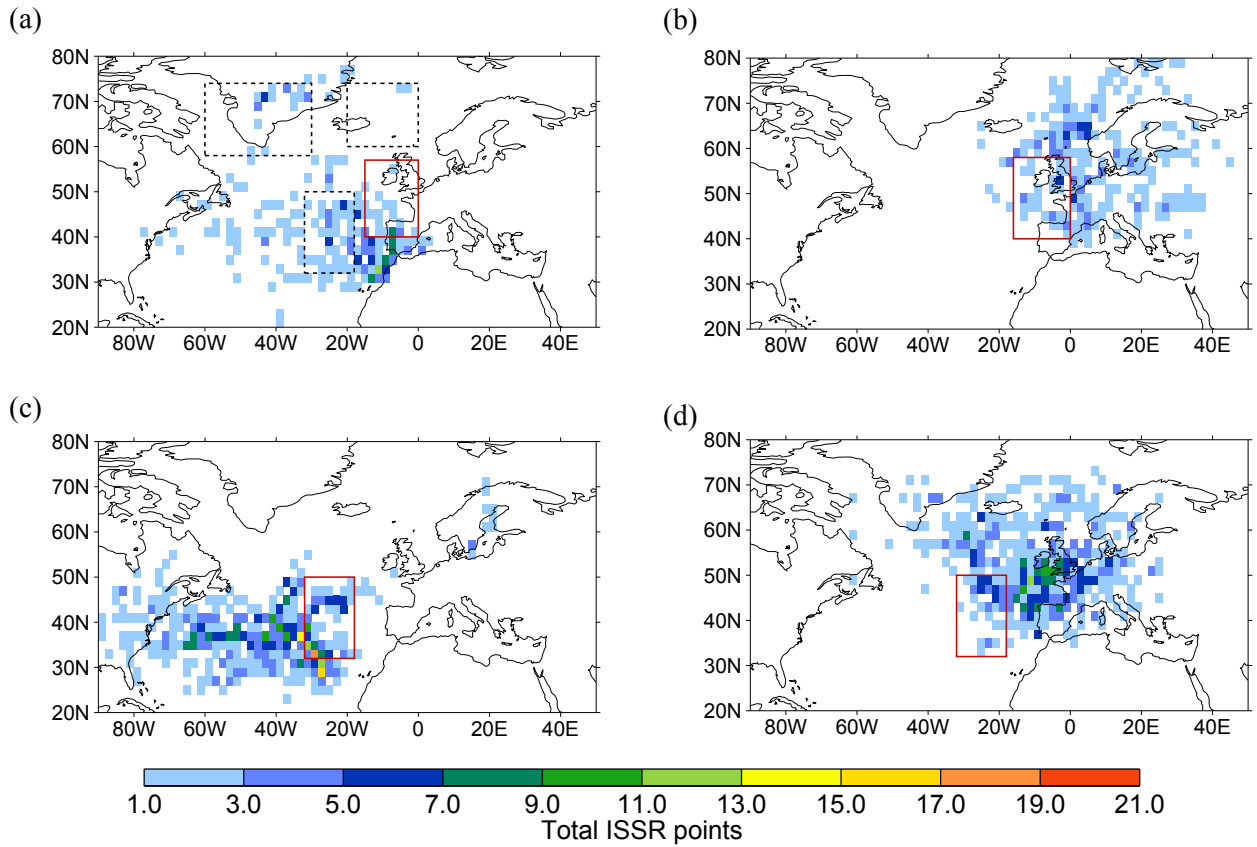


Figure 6. For ISS trajectories released from all levels in winter, whose the first point of ISS is within the Atlantic-European region (defined by the red box, top row) or mid-Atlantic region (bottom row), a density map of the location of this air (a, c) 24 h prior to, and (b, d) 24 h subsequent to this time. For tropospheric ISS air with an ISS lifetime of at least 24 h. The locations of all regions are marked as boxes on (a).

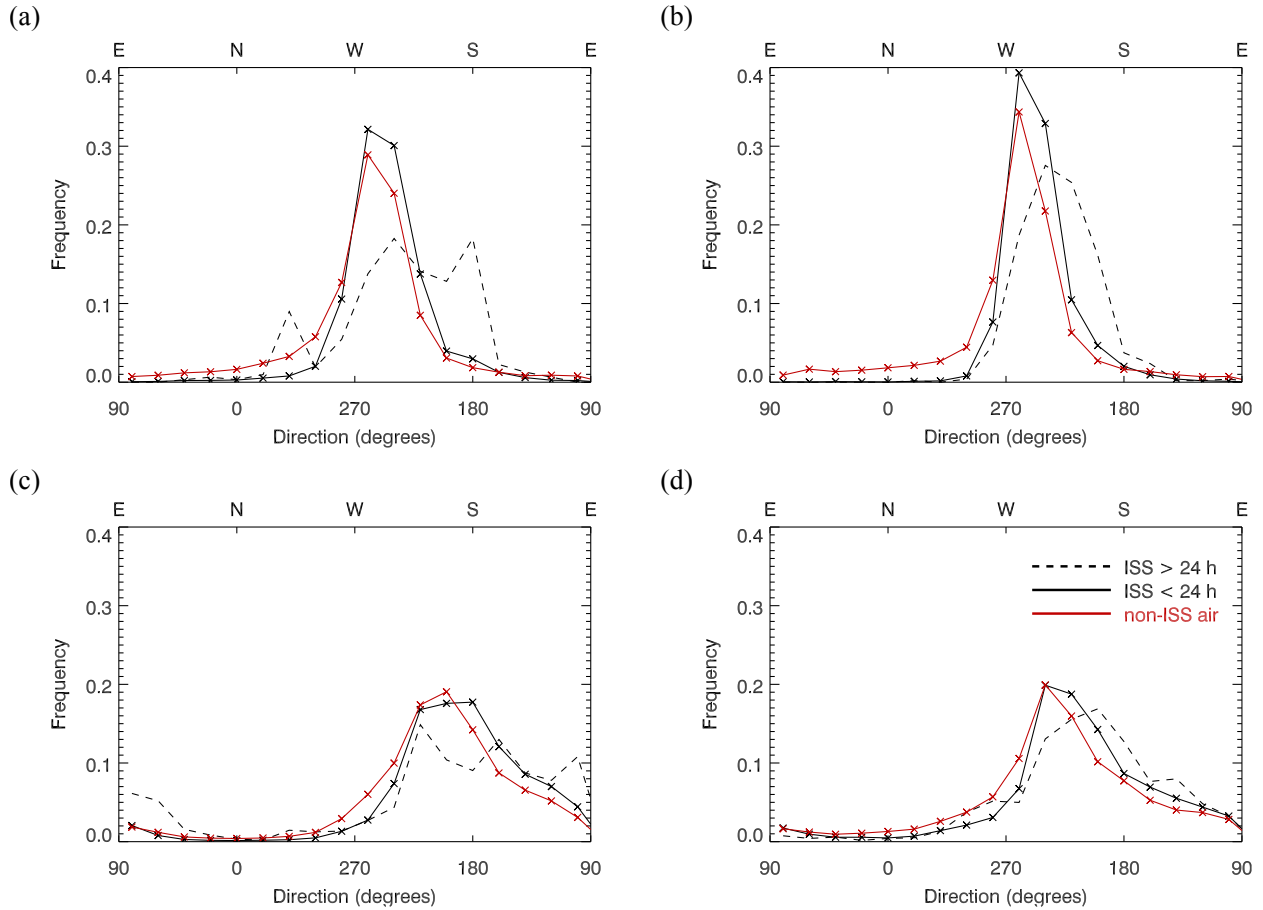


Figure 7. The direction of movement of air along a trajectory in the 24 h leading up to ISS, for regions (a) Atlantic-Europe in winter, (b) mid-Atlantic in winter, (c) Greenland in winter and (d) Iceland in summer, for trajectories released from all three levels. Shown for: tropospheric ISS air with a lifetime less than 24 h (black solid line), tropospheric ISS air with a lifetime of at least 24 h (black dashed line) and subsaturated air (red line).

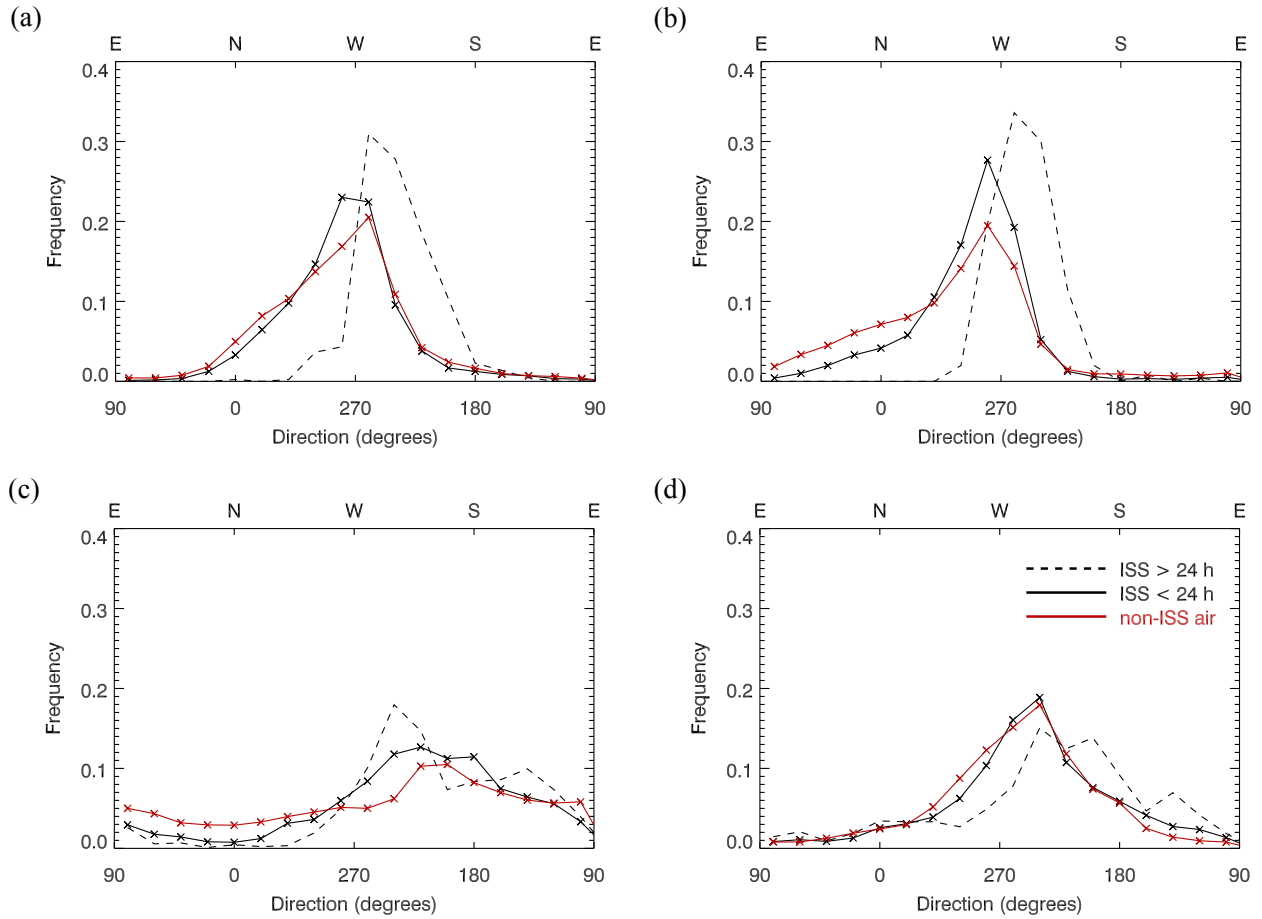


Figure 8. The direction of movement of air along a trajectory in the 24 h following the first point of ISS, for regions (a) Atlantic-Europe in winter, (b) mid-Atlantic in winter, (c) Greenland in winter and (d) Iceland in summer, for trajectories released from all three levels. Shown for: tropospheric ISS air with a lifetime less than 24 h (black solid line), tropospheric ISS air with a lifetime of at least 24 h (black dashed line) and subsaturated air (red line).